Candidate Population III stellar complex at z=6.629 in the MUSE Deep Lensed Field

E. Vanzella[1]*, M. Meneghetti[1], G. B. Caminha[2], M. Castellano[3], F. Calura[1], P. Rosati[4,1], C. Grillo[5], M. Dijkstra, M. Gronke[6], E. Sani[7], A. Mercurio[8], P. Tozzi[9], M. Nonino[10], S. Cristiani[10], M. Mignoli[1], L. Pentericci[3], R. Gilli[1], T. Treu[11], K. Caputi[2], G. Cupani[10], A. Fontana[3], A. Grazian[12] and I. Balestra[10,13]

[1] *INAF – Osservatorio di Astrofisica e Scienza dello Spazio, via Gobetti 93/3, 40129 Bologna, Italy*
[2] *Kapteyn Astronomical Institute, University of Groningen, Postbus 800, 9700 AV Groningen, The Netherlands*
[3] *INAF – Osservatorio Astronomico di Roma, Via Frascati 33, I-00078 Monte Porzio Catone (RM), Italy*
[4] *Dipartimento di Fisica e Scienze della Terra, Università degli Studi di Ferrara, via Saragat 1, I-44122 Ferrara, Italy*
[5] *Dipartimento di Fisica, Università degli Studi di Milano, via Celoria 16, I-20133 Milano, Italy*
[6] *Department of Physics, University of California, Santa Barbara, CA 93106, USA*
[7] *European Southern Observatory, Alonso de Cordova 3107, Casilla 19, Santiago 19001, Chile*
[8] *INAF – Osservatorio Astronomico di Capodimonte, Via Moiariello 16, I-80131 Napoli, Italy*
[9] *INAF – Osservatorio Astrofisico di Arcetri, Largo E. Fermi, I-50125, Firenze, Italy*
[10] *INAF – Osservatorio Astronomico di Trieste, via G. B. Tiepolo 11, I-34143, Trieste, Italy*
[11] *Department of Physics and Astronomy, University of California, Los Angeles, CA 90095, USA*
[12] *INAF – Osservatorio Astronomico di Padova, Vicolo Osservatorio 5, 35122, Padova, Italy*
[13] *OmegaLambdaTec GmbH, Lichtenbergstrasse 8, 85748 Garching bei Munchen, Germany*

ABSTRACT

We discovered a strongly lensed ($\mu \gtrsim 40$) Lyα emission at z=6.629 (S/N $\simeq$ 18) in the MUSE Deep Lensed Field (MDLF) targeting the Hubble Frontier Field galaxy cluster MACS J0416. Dedicated lensing simulations imply that the Lyα emitting region necessarily crosses the caustic. The arc-like shape of the Lyα extends 3″ on the observed plane and is the result of two merged multiple images, each one with a de-lensed Lyα luminosity L $\lesssim 2.8 \times 10^{40}$ erg s^{-1} arising from a confined region ($\lesssim$ 150 pc effective radius). A spatially unresolved HST counterpart is barely detected at S/N $\simeq$ 2 after stacking the near-infrared bands, corresponding to an observed(intrinsic) magnitude $m_{1500} \gtrsim 30.8(\gtrsim 35.0)$. The inferred rest-frame Lyα equivalent width is EW$_0$ > 1120Å if the IGM transmission is T$_{IGM}$ < 0.5. The low luminosities and the extremely large Lyα EW$_0$ match the case of a Population III star complex made of several dozens stars ($\sim 10^4$ M$_\odot$) which irradiate a H$_{II}$ region crossing the caustic. While the Lyα and stellar continuum are among the faintest ever observed at this redshift, the continuum and the Lyα emissions could be affected by differential magnification, possibly biasing the EW$_0$ estimate. The aforementioned tentative HST detection tend to favour a large EW$_0$, making such a faint Pop III candidate a key target for the James Webb Space Telescope and Extremely Large Telescopes.

Key words: galaxies: formation – galaxies: starburst – gravitational lensing: strong

1 INTRODUCTION

Finding and characterising the first galaxies is the next frontier in observational astronomy. It is thought that the Universe was initially metal-enriched by the first generation of Population III (Pop III) stars, that could also have played a key role in cosmic reionisation before the formation of primeval galaxies (e.g., Zackrisson, & Vikaeus 2019; Wise 2019; Dayal, & Ferrara 2018, and references therein). Late ($z < 7$) Pop III star formation might also have occurred in pristine regions due to inhomogeneous metal enrichment of the first galaxies (Tornatore, Ferrara & Schneider 2007; Visbal et al. 2016; Salvaterra et al. 2011). Given the exceptionally high effective temperatures of Pop III stars in

* E-mail: eros.vanzella@inaf.it

arXiv:2001.03619v2 [astro-ph.GA] 5 Mar 2020

the zero-age main sequence, they emit a large fraction of their luminosity in the Lyman continuum and have a much harder ionising spectrum than stars with higher metallicity. The main characteristics of their predicted spectral energy distribution (SED) are the presence of a prominent rest-fame Lyα (Lyman-alpha) emission line due to the strong ionising flux up to $\sim 1000 - 4000$Å rest-frame equivalent width (denoted as EW_0, hereafter) and significant He recombination line (especially HeIIλ1640, with EW_0 up to 15-40Å) due to spectral hardness, while a clear deficit of all the metal lines is expected. In particular, Inoue (2011) suggested the following criteria for the identification of extremely metal poor or Pop III galaxies: $EW_0(Ly\alpha) > 230$Å, $EW_0([OIII]5007)$ < 20Å and $EW_0(HeII\lambda1640) > 1$Å, and prominent Balmer lines like $EW_0(H\alpha) > 1900$Å, while showing an extremely blue ultraviolet spectral slope ($\beta \sim -3$, $F(\lambda) \sim \lambda^{\beta}$).

Observations have yielded candidates for Pop III stellar populations at high redshift (e.g., Kashikawa et al. 2012; Sobral et al. 2015, and references therein), yet without any definitive detection. These include a controversial $z = 6.6$ galaxy dubbed CR7 that displays HeIIλ1640 emission (Sobral et al. 2019; Shibuya et al. 2018). Thus, to date, there has not been a confirmed observation of a galaxy dominated by the flux of Pop III stars. The possibility of observing signatures from very metal poor or Pop III star clusters through gravitational lensing has also been discussed, e.g., Zackrisson et al. (2015) (see also Hernán-Caballero et al. 2017), including the detection of single Pop III stars with fluxes temporarily magnified to extreme values (with the magnification parameter $\mu \simeq 10^3 - 10^5$) during their transit across the caustic of a galaxy cluster. Such single−star−transit events can boost the flux of the star by $7 - 12$ mag (Windhorst et al. 2018), making such objects visible for a limited amount of time even down to intrinsic magnitudes of $35 - 38$. Examples of such events detecting single normal stars at $z < 2$ have been reported recently by Rodney et al. (2018).

Very low-luminosity emission line galaxies have been identified in Hubble Ultra Deep Field, down to magnitude $30 - 32$ (M_{1500} = -15) and S/N $\sim 1 - 5$ (Maseda et al. 2018). Strong gravitational lensing allowed us to shed further light on similar low-luminosity objects, providing higher S/N ~ 20 for individual cases (e.g., Vanzella et al. 2017, 2019). In this letter we present an object at z=6.629 showing (1) the faintest Lyα emission ever detected at $z > 6$ crossing the caustic of the Hubble Frontier Field (HFF) galaxy cluster MACS J0416 (Lotz et al. 2017) and (2) a large Lyα EW_0, potentially implying that extreme stellar populations are present. We assume a flat cosmology with $\Omega_M = 0.3$, $\Omega_\Lambda = 0.7$ and $H_0 = 70$ km s^{-1} Mpc^{-1}.

2   THE MUSE DEEP LENSED FIELD: MDLF

VLT/MUSE (Bacon et al. 2010) deep spectroscopic observations of 17.1 hours of integration time in a single pointing have been obtained on the HFF galaxy cluster MACS J0416 (Prog. `0100.A-0763(A)`, PI Vanzella). The data reduction follows the technique described in Caminha et al. (2017), eventually achieving a PSF with FWHM of 0.6″ in the final datacube. A more detailed description of the observational campaign of the MDLF and of the data reduction will be presented elsewhere. A refined lens model of HFF J0416 us-
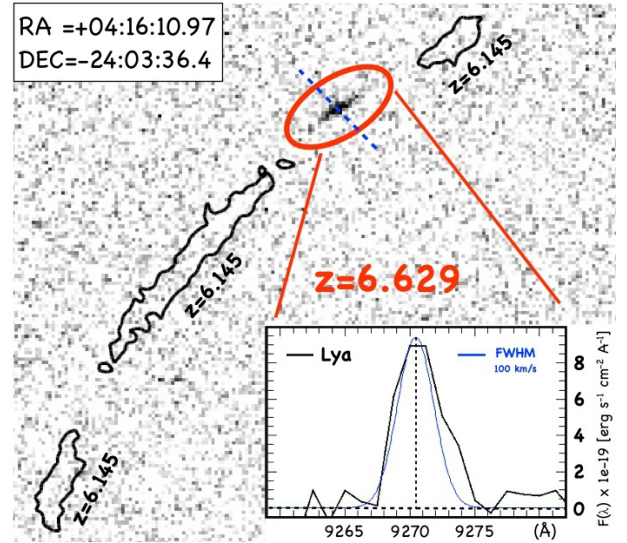

Figure 1. A $30'' \times 30''$ region extracted from the MDLF at the z=6.629 Lyα wavelength and averaged over $dv = 200$ km s^{-1}. The indicated Lyα arclet straddles the critical line (marked with the blue dotted line), close to a highly magnified system already confirmed at z=6.145 and well constrained by the three giant Lyα arcs (black contours). The one-dimensional spectrum of the Lyα line at z=6.629 is shown in the inset, where the asymmetry towards the red side is evident (a Gaussian with FWHM=100 km s^{-1} is superimposed with a blue line).

ing a new set of confirmed multiple images from the MDLF, will also be presented in a forthcoming paper.

2.1   A Lyα arc at z=6.629 and the faint HST counterpart

Figure 1 shows the extended (3″) arc from the continuum subtracted narrow band image extracted from the MUSE data cube and the one-dimensional profile of the emission line at $\lambda = 9270.7$Å, in a region free from OH sky emission lines. The arc is detected at S/N=18 with flux 4.4×10^{-18} erg s^{-1} cm^{-2} calculated within an elliptical aperture with major and minor axes of 4″ and 1.5″, respectively, and shows an asymmetric profile having an instrumental corrected FWHM of 98($\pm$7) km s^{-1}. We identify this line as Lyα at $z = 6.629$ for the following reasons: (1) the weighted skewness S_W (as defined by Shimasaku et al. 2006) is 3.4 ± 0.7, in line with the typical values observed for asymmetric Lyα emissions at high-z (it is zero for symmetric shapes, Figure 1); (2) if it is identified to other typical lines like [OII]λ3727, 3729, [OIII]λ4959, [OIII]λ5007, Hβ, or Hα, each of them would imply the presence and detection of additional lines in the same spectrum; (3) the MUSE spectral resolution at $\lambda > 9000$Å is $R \simeq 3500$, high enough to resolve the single components of the doublets like CIVλ1548, 1550, OIII]λ1661, 1666, CIII]$\lambda\lambda$1907, 1909, [OII]λ3727, 3729 further excluding these lines for identification. As Figure 2 shows, there is no clear detection in the F105W (Y), F125W (J), F140W (JH), and F160W (H) bands in the HFF images, probing the ultraviolet stellar continuum down to the nominal depth of the HFFs (mag $\simeq$ 29, at 5σ limit Lotz et al. 2017). We therefore computed the Y+J+JH+H weighted-mean stacked images
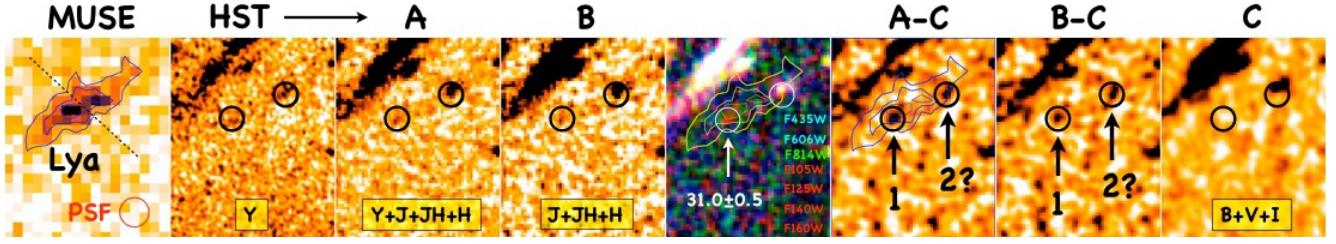
Figure 2. From left to right: the MUSE Lyα emission averaged over $dv = 160$ km s^{-1} (the 2 and 4 σ contours are shown, with the dotted line marking the critical line); the Y-band HST image; the stacked Y+J+JH+H and J+JH+H images with indicated the positions of the two possible high-z counterparts (solid circles with diameter 0.4″); the colour stacked image; the differential stacked HST images highlighting the two possible counterparts (A-C) and (B-C) after a Gaussian smoothing with σ=1 pix; the B+V+I stacked image (C).

(probing $\lambda \sim 1500$Å), reaching a 1σ limit of 31.6 within circular apertures of diameter 0.4″. Such a limit has been derived by inserting 30 apertures in free regions surrounding the source position and computing the standard deviation among them (the A-PHOT tool has be used for this task, Merlin et al. 2019). As discussed in the next section, there is a configuration in which we expect the presence of two very close multiple images near the Lyα arc. Indeed, there is a possible detection at S/N ~ 2 lying within the arclet indicated as 1 in Figure 2, with $m_{1500} \simeq 31$ and showing a photometric drop in the F435W+F606W+F814W image. The same test has been performed adopting an elliptical aperture oriented along the arc, with semi-axis 0.7″ and 0.2″, and no signal has been detected down to $m_{1500} \simeq 30.85$ at 1σ. We expect a second nearby image with similar magnification that, however, is contaminated by a foreground object clearly detected in the blue bands. While image 1 could be the HST counterpart, a tentative second image detection marked as 2 is shown in Figure 2.

3 THE Lyα EMISSION IS ON THE CAUSTIC

The Lyα arc lies in a well known region of the galaxy cluster where Vanzella et al. (2017, 2019) already discussed another star-forming complex system at z=6.145 showing several multiple images identified in deep HST data, producing three clear Lyα arcs in the MUSE observations (Figure 1). The presence of such a system adds valuable constraints for the case studied in this work. In fact, any detection at $z > 6$ in the region where the z=6.629 arc lies, would produce multiple images as in the case observed at z=6.145, unless such images are so close to merge into a single spatially unresolved mildly elongated arc. It is exactly the case for the z=6.629 arclet discussed here: the absence of two distinct images (Figure 1 and 2) implies that the Lyα arc straddles the critical line and is indeed the result of two spatially unresolved Lyα images, generated by a Lyα emitting region lying on the corresponding caustic.

3.1 Simulating the caustic crossing

In order to perform a quantitative estimate of the magnification of the Lyα emission, we use dedicated simulations with a customised version of the software SkyLens (e.g. Meneghetti et al. 2010; Plazas et al. 2019). The method will be extensively described in a future paper. In short, we perform the following steps. We start from the assumption that the
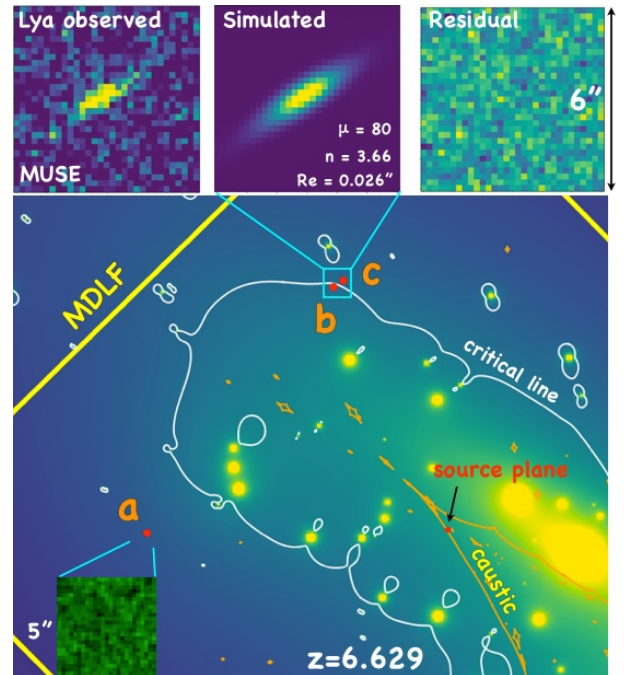

Figure 3. The tangential caustic (orange) and the critical line (white) are superimposed to the (false-colour) image of the galaxy cluster members used for the strong lensing model. The observed Lyα arc is well reproduced when the source is very close to the caustic (black arrow). Three multiple images are predicted (marked as a, b and c): images b,c merge into a single small arc, whereas image a is not detected (bottom-left inset). In the top panels, the observed, simulated and residuals Lyα images are shown for the best fit values of n, R_e and $\mu = \mu(a) + \mu(b)$.

source of the Lyα emission can be described by a single, circularly symmetric Sérsic surface brightness profile. The profile is characterised by the Sérsic index n and by the effective radius R_e. We ray-trace 2000×2000 light rays through a squared region containing the Lyα emission (cyan square in Figure. 3, whose size is $\sim 6.2'' \times 6.2''$) and propagate them towards the source plane at redshift $z_s = 6.629$, accounting for the deflections induced by the lensing cluster. In this work, we use the strong lensing model described in Caminha et al. (2017)[1]. On the source plane, the arrival

---

[1] The LensTool model is published in the HFF lens model format at *http://www.fe.infn.it/astro/lensing/*

positions of the light rays are used to sample the brightness distribution of the source, which is then mapped onto the image plane. By performing this operation, we reconstruct the lensed image, which is subsequently convolved with a Gaussian PSF with a FWHM of 0.6". The resulting convolved image is first rebinned at the same resolution of the MUSE image ($0.2''$/pixel) and then compared to the observed Lyα arclet. We use the python package LMfit to perform a Non-linear Least Square Minimisation of a cost function defined as the squared difference between the simulated and the observed images. As shown in the upper panels of Figure. 3, the source model, despite its simplicity, reproduces very well the observed arclet morphology. The two parameters n and R_e are quite degenerate. For a Sérsic index in the range $n = 1 - 4$, the best fit effectitve radius R_e varies between $0.012'' - 0.027''$. The best fit solution corresponds to $n = 3.66$ and $R_e = 0.026''$. The latest is equivalent to 140 pc on the source plane. In all cases, the model suggests that the Lyα emitting region partially overlaps with the caustic, meaning that only part of the source is reproduced twice in the arclet.

Having obtained a model for the Lyα source, we can estimate the magnification of the arclet by comparing the lensed and the intrinsic fluxes of the source after integrating the surface brightness over the region used for ray-tracing. We estimate that the total magnification of the Lyα arclet (images b and c) is $\mu(b+c) = \mu(b) + \mu(c) \simeq 80$, implying that the de-lensed Lyα flux of the arclet is $\sim 5.5 \times 10^{-20}$ erg s^{-1} cm^{-2}. Keeping $n \sim 1$ (exponential profile) in our fitting procedure the magnification increases to $\mu(b+c) \sim 110$.

It is well known that such magnification estimate is prone to systematic errors due to the uncertainties of the lens model in regions where the magnification gradients are very strong (e.g., Meneghetti et al. 2017). In order to circumvent this limitation, we can make use of the counter image a, which is predicted to form much farther from the critical lines (Figure. 3). Using our best fit source determined above, we estimate that $\mu(a) \sim 4.5$ with an uncertainty smaller than 20%. We also find that, because of the much shallower magnification gradient in this region, the estimate is quite insensitive to the properties of the source. Indeed, $\mu(a)$ would change by $\sim 5\%$ ($\mu(a) \sim 4.3$) by adopting a point source approximation. The image a is not detected at the depth of the MDLF down to 1σ Lyα flux limit $f_{a,lim}$ ($\sim 2.4 \times 10^{-19}$ erg s^{-1} cm^{-2}, for a point-like source, consistently to Inami et al. 2017). This sets a lower limit $\mu(b+c) \gtrsim \mu(a)f_{bc}/f_{a,lim}$, where the observed ratio is $f_{bc}/f_{a,lim} \simeq 18$. Therefore, we can conclude that $\mu(b+c) \gtrsim 80$, in keeping with the fitting procedure ($\mu = 80 - 110$).

3.2 A large Lyα EW

The computation of the EW of the Lyα line (L) requires an estimate of the underlying stellar continuum (S), taking into account that magnifications associated to S (μ_S) and L (μ_L) might differ. A general expression for EW$_0$ is:

$$EW_0 = \frac{1}{(1+z)} \frac{\mu_S}{\mu_L} \frac{f(\mathrm{Ly}\alpha)}{F_\lambda(UV) \times T_{IGM}(\mathrm{Ly}\alpha)} , \qquad (1)$$

where $f(\mathrm{Ly}\alpha)$ is the Lyα flux (5.5×10^{-20} erg s^{-1} cm^{-2}), $F_\lambda(UV)$ is the ultraviolet continuum at the Lyα wavelength for which we assume a value $< 1.27 \times 10^{-23}$ erg s^{-1} cm^{-2}Å^{-1}, corresponding to $m_{1500} \gtrsim 35$ (=

$31 + 2.5 \mathrm{Log}_{10}(\mu)$, $\mu \gtrsim 40$). Given the large uncertainties on the HST detection (S/N ~ 2, $\sigma_m \sim 0.5$), any assumption on the ultraviolet slope β would not be significant. Indeed, a slope $\beta = -2.5$ (-3) would imply a magnitude difference of $m_{1216} - m_{1500} = -0.11$ (-0.23). $T_{IGM}(\mathrm{Ly}\alpha)$ is the transmission of the intergalactic medium for Lyα photons (see below, and Table 1). We identify two scenarios:

• if we assume that L and S have the same intrinsic size and brightness profile, then $\mu_S \simeq \mu_L$ and the EW$_0$ is independent on the lens model. Thus, under this assumption, a lower limit on EW$_0$ can be found by using the very low significance detection (if not the non-detection) of the UV continuum, $m_{1500} \gtrsim 35$. Combined with the de-lensed Lyα flux of 5.5×10^{-20} erg s^{-1} cm^{-2} leads to the result that EW$_0 > 564$Å, in the case $T_{IGM}(\mathrm{Ly}\alpha) = 1.0$. The low significance of the HST detection prevents us from verifying whether S is extended as the arclet.

• if, in contrast, we assume that the size of S is smaller than that of L, as it might be the case when S is embedded and generates the H II region (e.g., Steidel et al. 2011), then we expect that $\mu_S > \mu_L$ and consequently EW$_0$ would be even larger than in the previous case.

There is still the possibility that S is located outside the lens caustic. In this scenario no continuum flux is expected near the Lyα arclet. We could only use the non-detection in the HST data of image a ($m > 31.6$ at 1σ), where S is certainly present, to set an upper limit of $F_\lambda(UV)$. Using the fact that $\mu(a) \sim 4.5$, the de-lensed magnitude limit is $m > 33.2$. Combined with the lower limit of the magnification of L ($\mu_L \gtrsim 80$), we obtain that EW$_0 \gtrsim 110$Å in the case $T_{IGM}(\mathrm{Ly}\alpha) = 1.0$. Note, however, that the marginal detection of image 1 in the stacked HST images (see Figure 2), which could be the image of S, seems to disfavour this scenario.

It is now worth discussing the IGM transmission $T_{IGM}(\mathrm{Ly}\alpha)$ which depends on *both* the "intrinsic" (pre-IGM) Lyα spectrum emerging *and* the IGM properties. Due to the resonant absorption of the neutral or partially neutral IGM combined with cosmological inflow, the Lyα spectrum blueward of $v_{\mathrm{cutoff}} \lesssim 200$km s^{-1} is absorbed (Dijkstra, & Wyithe 2007). Thus, the more asymmetric the intrinsic Lyα is towards the blue or the lower the red peak offset from systemic, the lower T_{IGM}. All this implies that T_{IGM} is highly uncertain and estimates reach from tens of percent (e.g., $T_{IGM} = 0.20^{+0.12}_{-0.15}$ at $z = 6.6$, Laursen et al. 2011) to values approaching unity for an intrinsic single read peak with offset > 300 km s^{-1}. However, since the Lyα spectrum presented here is very narrow and asymmetric (cf. Sect. 2.1) it is likely that either a significant part of the red peak has been removed from the IGM (in case of an intrinsic spectrum with a large offset, and thus, large width), or an intrinsic blue component existed (in the case of a small intrinsic offset). Both cases would imply a significant absorption of the IGM, and hence, $T_{IGM} < 1$. Knowledge of the systemic redshift, through, e.g., Hα information would be helpful in reconstructing the intrinsic Lyα line, and thus, to constrain T_{IGM} more qualitatively. This could, furthermore, rule out the radiative transfer effects as an origin of the large EW – which we already deem unlikely due to the asymmetry of the observed line.

We conclude that, even assuming $T_{IGM}(\mathrm{Ly}\alpha) = 1$, a still quite extreme EW$_0$(Lyα) > 550Å emerges from a region crossing the caustic, that can easily approach (or exceed)

Table 1. Properties of the Lyα emitter in the source plane.

Lyα [erg s^{-1} cm^{-2}]	5.5×10^{-20}
Lyα [erg s^{-1}]	2.8×10^{40}
EW$_0$(Lyα) [Å] (T$_{\mathrm{IGM}} < 0.5$)	> 1120
M$_{1500}$(m_{1500}) (2σ)	$\gtrsim -11.9$ ($\gtrsim 35$)
R_e Lyα region [pc]	< 150
Magnification [$\mu(b) = \mu(c)$]	$\mu(b) + \mu(c) \gtrsim 80$; $\mu(a) \simeq 4.5$

1000Å assuming a more plausible T$_{\mathrm{IGM}}$(Lyα) < 1.0. Though not totally excluded, we do not consider in this work the possibilities that the large EW(Lyα) originates from a very faint AGN (e.g., with BH mass of 10^{2-3} M$_\odot$, Fan 2012) or a multiphase scattering medium (e.g., Neufeld 1991).

4 CANDIDATE POP III STARS

The predicted EW$_0$(Lyα) for metal free stellar populations exceeds 400Å and it goes up to a few thousands rest-frame (Inoue 2011; Schaerer 2013), and is observable if neighbouring sources (either Pop III or Pop II stars) have already contributed toward ionising a local bubble (Sobral et al. 2015). The large EW$_0$(Lyα) value reported in this work opens for a possible dominant contribution by extremely metal poor stars. It is interesting to calculate how many Pop III stars are needed to reproduce both the observed M$_{1500}$ and L(Lyα):

• *UV continuum*: the apparent magnitudes at 1500Å rest-frame at $z = 7$ for Pop III star at ZAMS with masses $1-1000$ M$_\odot$ are reported by Windhorst et al. (2018). In particular, stars with masses of 100, 300, and 1000M$_\odot$ have magnitudes $m_{1500} = 40.08$, 38.64, and 37.44, respectively, neglecting dust attenuation. Adopting $m_{1500} \gtrsim 35$ (M$_{\mathrm{UV}} \gtrsim -11.9$, Sect. 3.2) and assuming for simplicity the same masses for all stars, the number of Pop III stars required to reproduce the intrinsic UV flux corresponding to M$_{\mathrm{UV}}$ amounts to N(M$_{\mathrm{UV}}$) = 10, 30, and 110 for stellar masses of 1000, 300 and 100M$_\odot$.

• *Lyα emission*: Mas-Ribas et al. (2016) provide the photon flux Q(H$_{\mathrm{I}}$)[s^{-1}] for different Pop III ZAMS stars and the conversion to L(Lyα) luminosity considering case-B departure, stochastic sampling of the Salpeter and Top-Heavy IMFs and zero escape fraction of the Lyman continuum radiation (note, however, that if a fraction of the ionising radiation escapes, the emerging Lyα would be dimmed linearly by the same factor, e.g., Schaerer 2013). We perform the calculation as above, assuming again the same mass for all stars (no boosting from the stochastic sampling of the IMF is considered). The Lyα luminosity emerging from Pop-III stars of mass 1000, 300, and 100 M$_\odot$ are 3.20×10^{40}, 8.11×10^{39}, and 1.72×10^{39} erg s^{-1}. Under the assumption that N(Lyα) = N(M$_{\mathrm{UV}}$) (being Lyα and M$_{\mathrm{UV}}$ referring to the same star complex), the resulting T$_{\mathrm{IGM}}$(Lyα) are 0.09, 0.11, and 0.16, respectively. These values double if the case-B is assumed, i.e., the predicted L(Lyα) is about a factor two fainter (Mas-Ribas et al. 2016). With such values of T$_{\mathrm{IGM}}$(Lyα) the resulting EW$_0$(Lyα) ranges between 4000-1500Å, for the three classes of Pop III stellar masses.

Future facilities are necessary to make a significant step forward. First, only the James Webb Space Telescope will access the optical rest-frame looking for the possible deficit of metals and the expected enormous Balmer emissions

(e.g., Inoue 2011), eventually gaining in depth with respect HST imaging. The next generation of Extremely Large Telescopes will also investigate the currently vague stellar component S by performing very deep imaging, while spectroscopy will address the deficiency of high-ionisation metal lines and the possible key HeIIλ1640 emission. The intrinsic HeIIλ1640/Lyα line ratio predicted for Pop III spans the range 0.01-0.10 (e.g., Schaerer 2013; Mas-Ribas et al. 2016), implying the expected flux of HeIIλ1640 would be $1.1 \times (10^{-21} - 10^{-20})$/T$_{\mathrm{IGM}}$(Lyα) erg s^{-1} cm^{-2}, clearly requiring an ELT-like telescope or an 8-10m class telescope in the most optimistic cases (T$_{\mathrm{IGM}}$(Lyα) $\ll 1$).

REFERENCES

Bacon, R., Accardo, M., Adjali, L., et al. 2010, Proc. SPIE, 7735, 773508
Caminha, G. B., Grillo, C., Rosati, P., et al. 2017, A&A, 600, A90
Dayal, P., & Ferrara, A. 2018, Phys. Rep., 780, 1
Dijkstra, M., & Wyithe, J. S. B. 2007, MNRAS, 379, 1589
Dijkstra, M. 2016, Understanding the Epoch of Cosmic Reionization: Challenges and Progress, 145
Fan, X. 2012, Research in Astronomy and Astrophysics, 12, 865
Hernán-Caballero, A., Pérez-González, P. G., Diego, J. M., et al. 2017, ApJ, 849, 82
Inami, H., Bacon, R., Brinchmann, J., et al. 2017, A&A, 608, A2
Inoue, A. K. 2011, MNRAS, 415, 2920
Laursen, P., Sommer-Larsen, J., & Razoumov, A. O. 2011, ApJ, 728, 52
Kashikawa, N., et al. 2012, ApJ, 761, 85
Lotz, J. M., et al. 2017, ApJ, 837, 97
Maseda, M. V., Bacon, R., Franx, M., et al. 2018, ApJ, 865, L1
Mas-Ribas, L., Dijkstra, M., & Forero-Romero, J. E. 2016, ApJ, 833, 65
Meneghetti, M., Rasia, E., Merten, J., et al. 2010, A&A, 514, A93
Meneghetti, M., Natarajan, P., Coe, D., et al. 2017, MNRAS, 472, 3177
Merlin, E., Pilo, S., Fontana, A., et al. 2019, A&A, 622, A169
Neufeld, D. A. 1991, ApJ, 370, L85
Plazas, A. A., Meneghetti, M., Maturi, M., et al. 2019, MNRAS, 482, 2823
Rodney, S. A., et al. 2018, Nature Astronomy, 2, 324
Salvaterra, R., Ferrara, A., & Dayal, P. 2011, MNRAS, 414, 847
Schaerer, D. 2013, The First Galaxies, Astrophysics and Space Science Library, Volume 396, 345
Shibuya, T., Ouchi, M., Harikane, Y., et al. 2018, PASJ, 70, S15
Shimasaku, K., Kashikawa, N., Doi, M., et al. 2006, PASJ, 58, 313
Sobral, D., Matthee, J., Darvish, B., et al. 2015, ApJ, 808, 139

Sobral, D., Matthee, J., Brammer, G., et al. 2019, MNRAS, 482, 2422

Steidel, C. C., Bogosavljević, M., Shapley, A. E., et al. 2011, ApJ, 736, 160

Tornatore, L., Ferrara, A., & Schneider, R. 2007, MNRAS, 382, 945

Vanzella, E., et al. 2017, MNRAS, 467, 4304

Vanzella, E., et al. 2019, MNRAS, 483, 3618

Visbal, E., Haiman, Z., & Bryan, G. L. 2016, MNRAS, 460, L59

Wise, J. H. 2019, arXiv e-prints, arXiv:1907.06653

Windhorst, R. A., et al. 2018, ApJS, 234, 41

Zackrisson, E., González, J., Eriksson, S., et al. 2015, MNRAS, 449, 3057

Zackrisson, E., & Vikaeus, A. 2019, arXiv e-prints, arXiv:1903.12555